

Figure 1: Seasonal June-August (JJA) average of precipitation for 1990-1991: a) from Experiment B1 with weak re-evaporation, contours are drawn for 1.0, 2.0, 4.0, 8.0, and 16.0 mm d^{-1} ; b) as (a) except for Experiment B2 (moderate re-evaporation); c) as (a) except for Experiment B3 (strong re-evaporation); d) as (a) except for Xie-Arkin precipitation data.

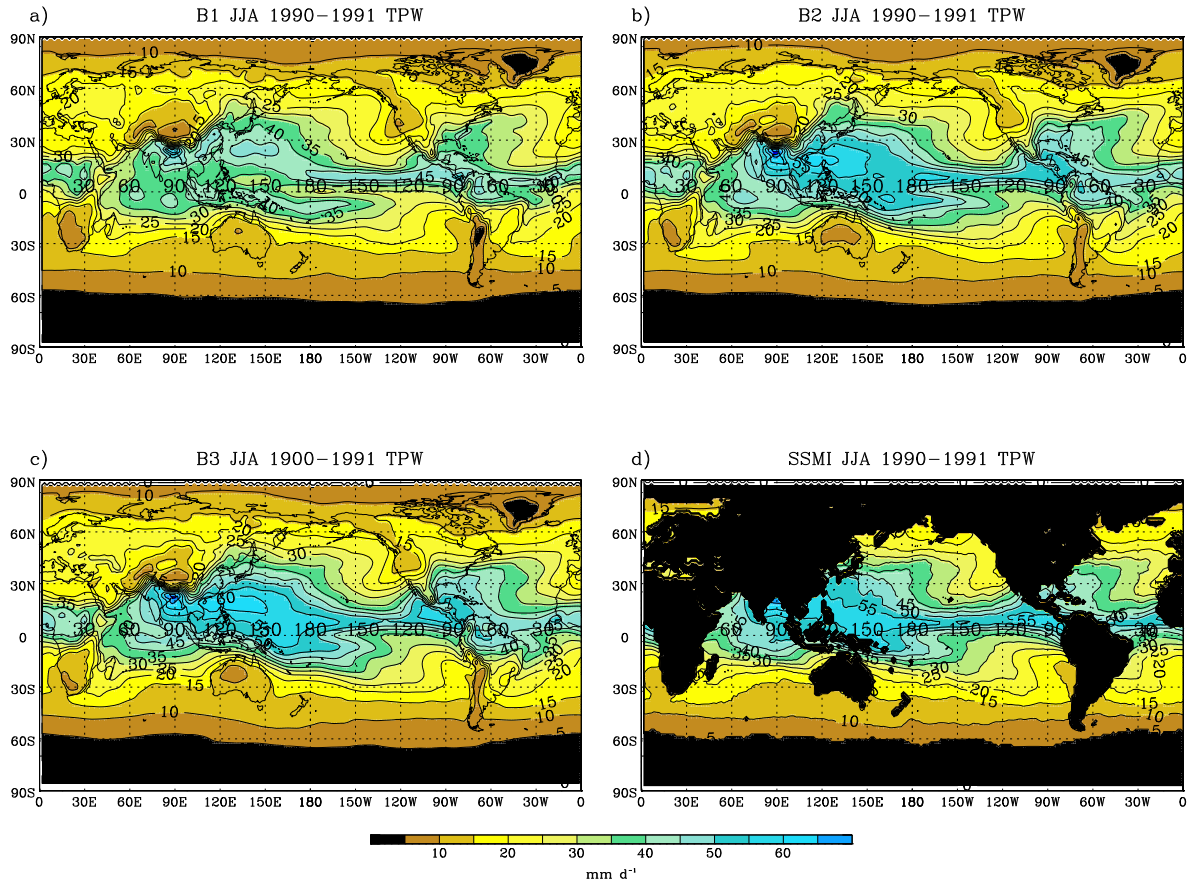


Figure 2: Total precipitable water for JJA 1990-1991 as a function of latitude and longitude: a) Experiment B1 (weak re-evaporation); b) Experiment B2 (moderate re-evaporation); c) Experiment B3 (strong re-evaporation); d) SSMI observational estimate. Contour interval is 5 kg m^{-2}

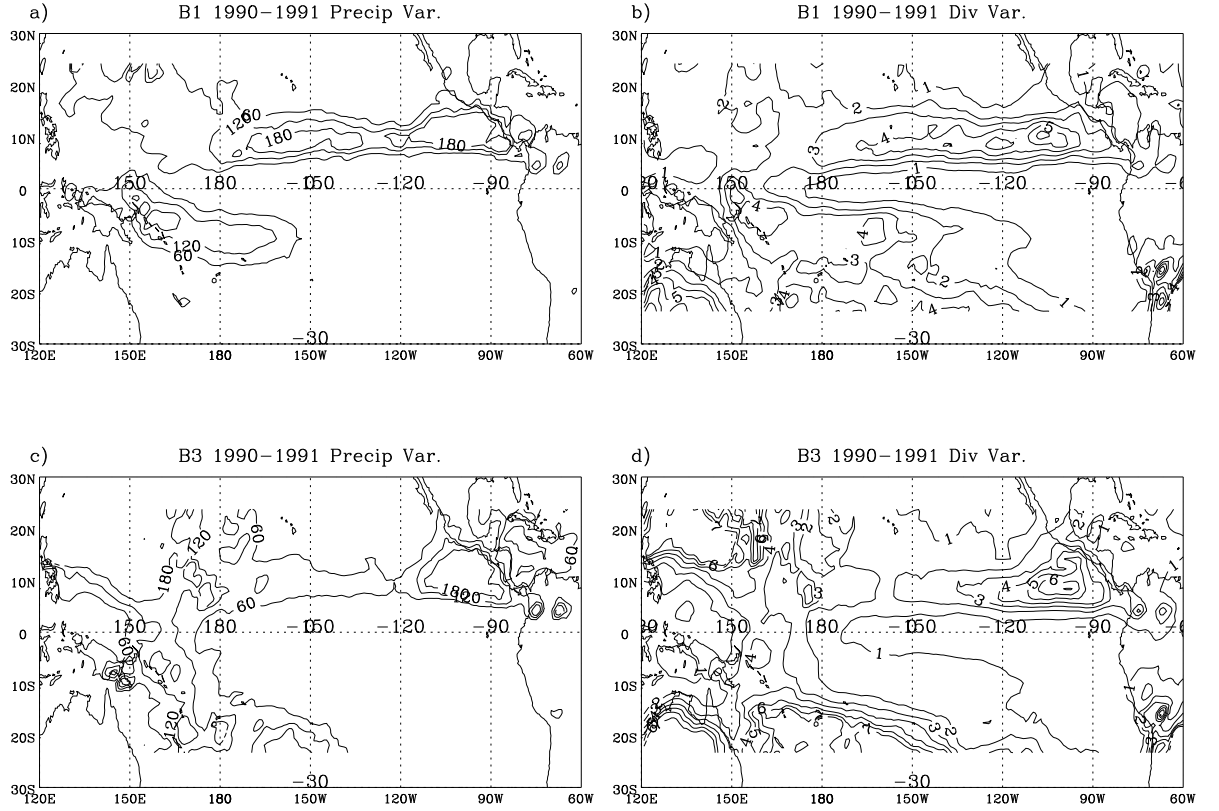


Figure 3: Mean variance of precipitation; (a) Exp B1, (c) Exp B3, and of integrated PBL convergence; (b) Exp B1, and (d) Exp B3, from transient disturbances with time scales less than 31 d. Mean variances are calculated for two northern warm seasons, i.e., May–October, 1990–1991. Contour interval in (a) and (c) is $60 \text{ mm}^2 \text{ d}^{-2}$, and in (b) and (d) is $1 \times 10^{-7} \text{ mb}^2 \text{ s}^{-2}$.

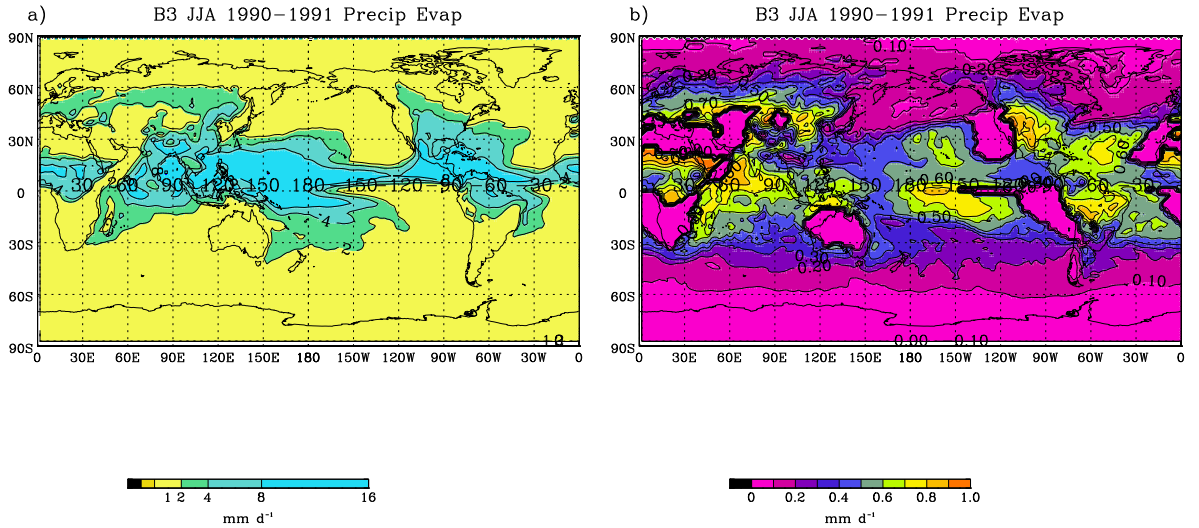


Figure 4: a) Mass-weighted, vertical integral of rain re-evaporation $\langle \mathcal{R} \rangle$ for JJA 1990-1991 in Experiment B3 (strong re-evaporation) as a function of latitude and longitude. Units are mm d^{-1} as for precipitation. Contour levels are 1.0, 2.0, 4.0, 8.0, and 16.0 mm d^{-1} as in Figures 1-4. b) Ratio of $\langle \mathcal{R} \rangle$ to total precipitation generated, i.e., \mathcal{P}_g , where \mathcal{P}_0 is the precipitation flux at the surface. Values over 0.5 imply that over half of the rain water generated by the model evaporates before reaching the surface.

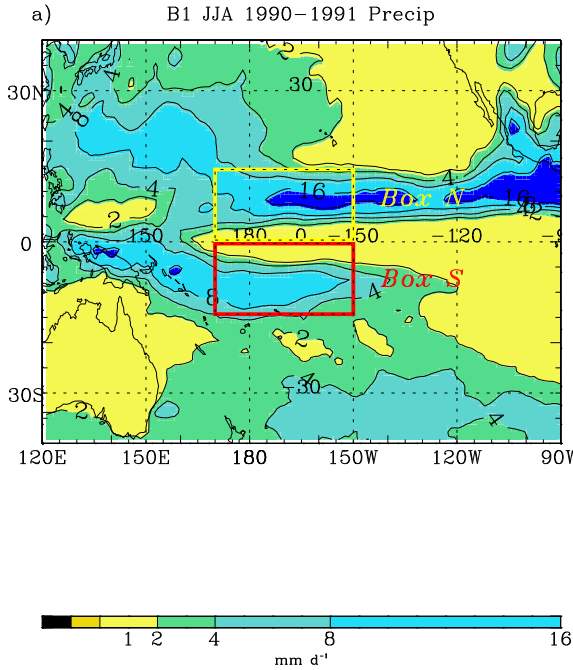


Figure 5: Domains used for profile and water budget analyses, shown over precipitation fields for JJA 1990-91 from Exp B1. The thick red line shows “Box S”, which is bounded by 170°E on the west, 150°W on the east, 14°S on the south and by the Equator on the north. It contains a significant portion of the spurious southern ITCZ that forms with weak re-evaporation. Box N is bounded by 170°E , 150°W in the zonal direction and by the Equator and 14°N in the meridional.

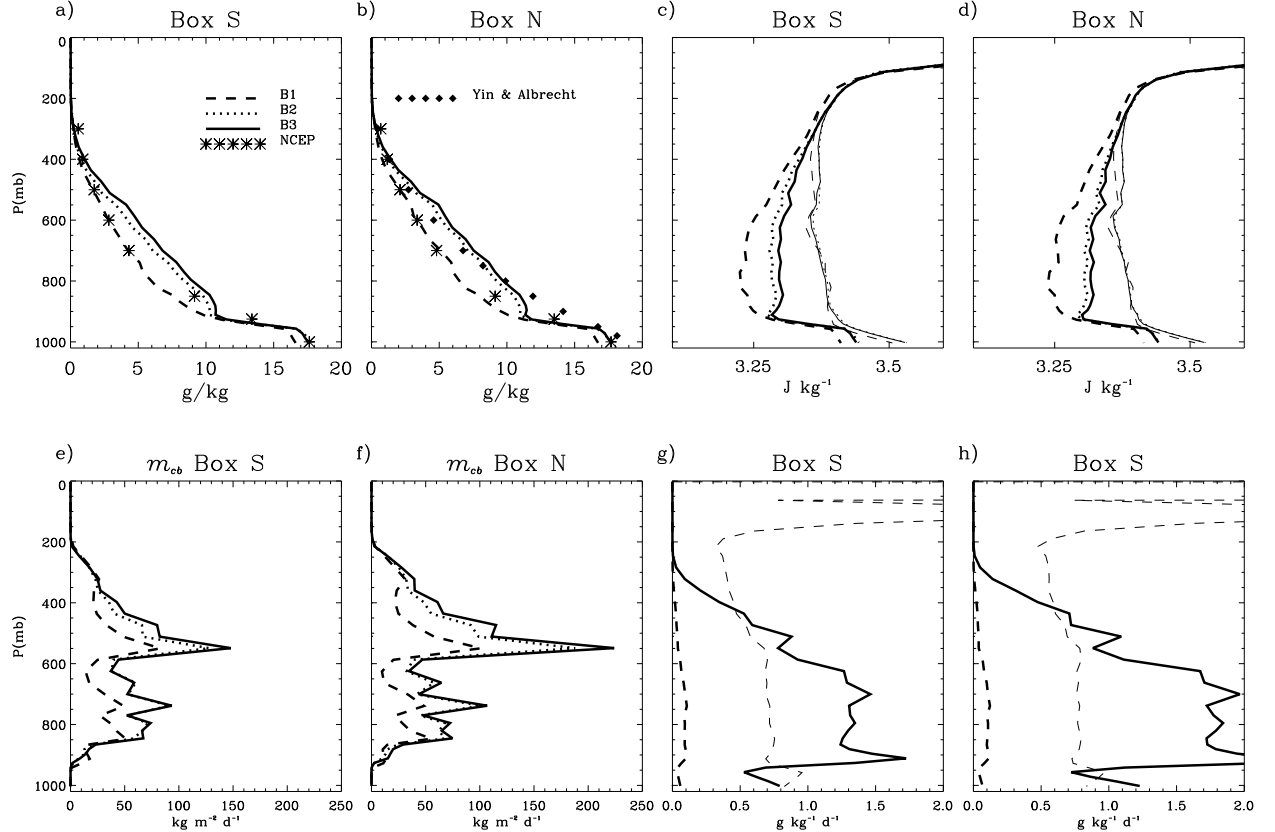


Figure 6: Box averaged profiles of; (a-b) specific humidity q , (c-d) moist static energies h and h^* , (e-f) cloud-base cumulus mass flux m_{cb} as a function of detrainment pressure, and (g-h) re-evaporation moistening tendency \mathcal{R} . Profiles for Box S (a,c,e,g), and Box N (b,d,f,h) are shown separately. In all panels Dashed lines indicate profiles for Exp B1, dotted lines for B2, and solid lines for B3. The “*” symbols in (a-b) show the NCEP re-analysis q profiles for the same period. Diamonds in (b) indicate aircraft derived water vapor profile from Yin and Albrecht 2000.

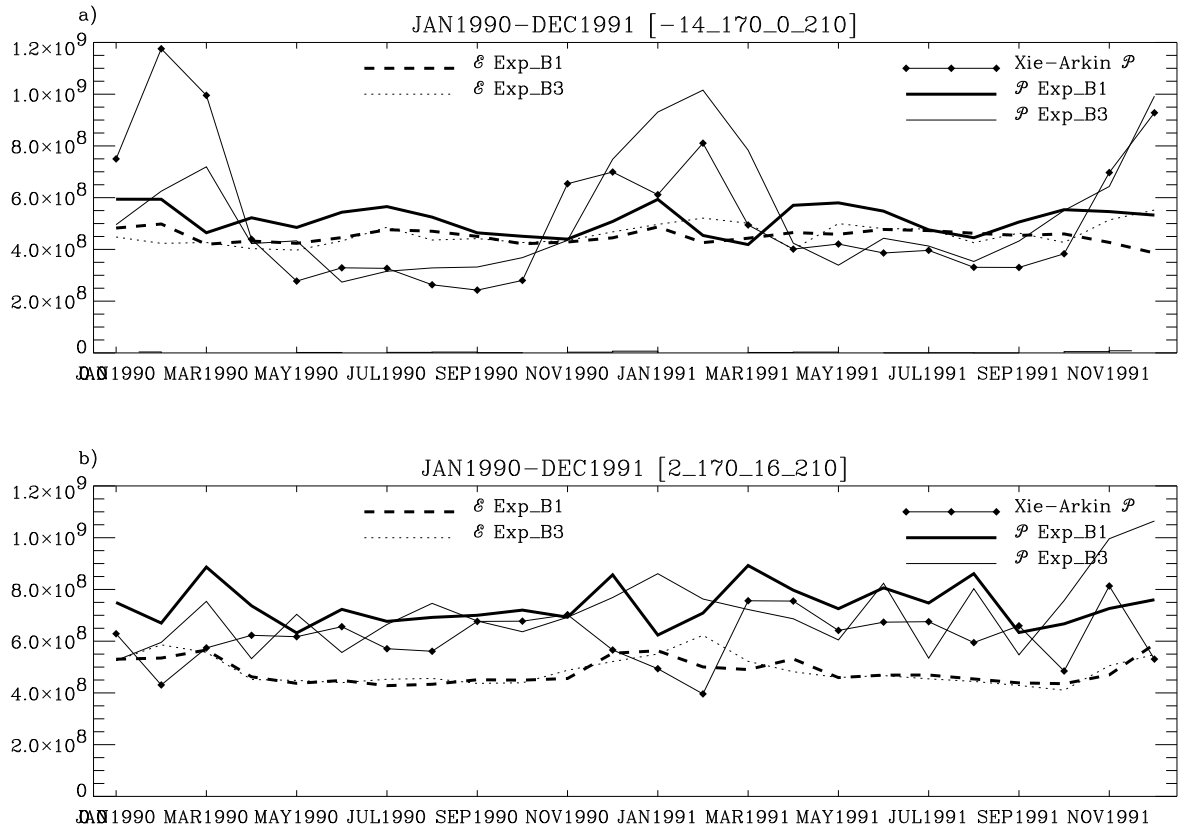


Figure 7: Monthly mean surface water vapor fluxes for; (a) Box S, and (b) Box N. Thick solid lines show total surface precipitation fluxes $\overline{\mathcal{P}_0}$ (kg s^{-1}) for Exp B1 and thin solid lines show $\overline{\mathcal{P}_0}$ for Exp B3. Thick dashed lines show total surface evaporation $\overline{\mathcal{E}_0}$ for B1, and thin dashed line for B3. Diamond symbols show total CMAP precipitation fluxes in both regions.

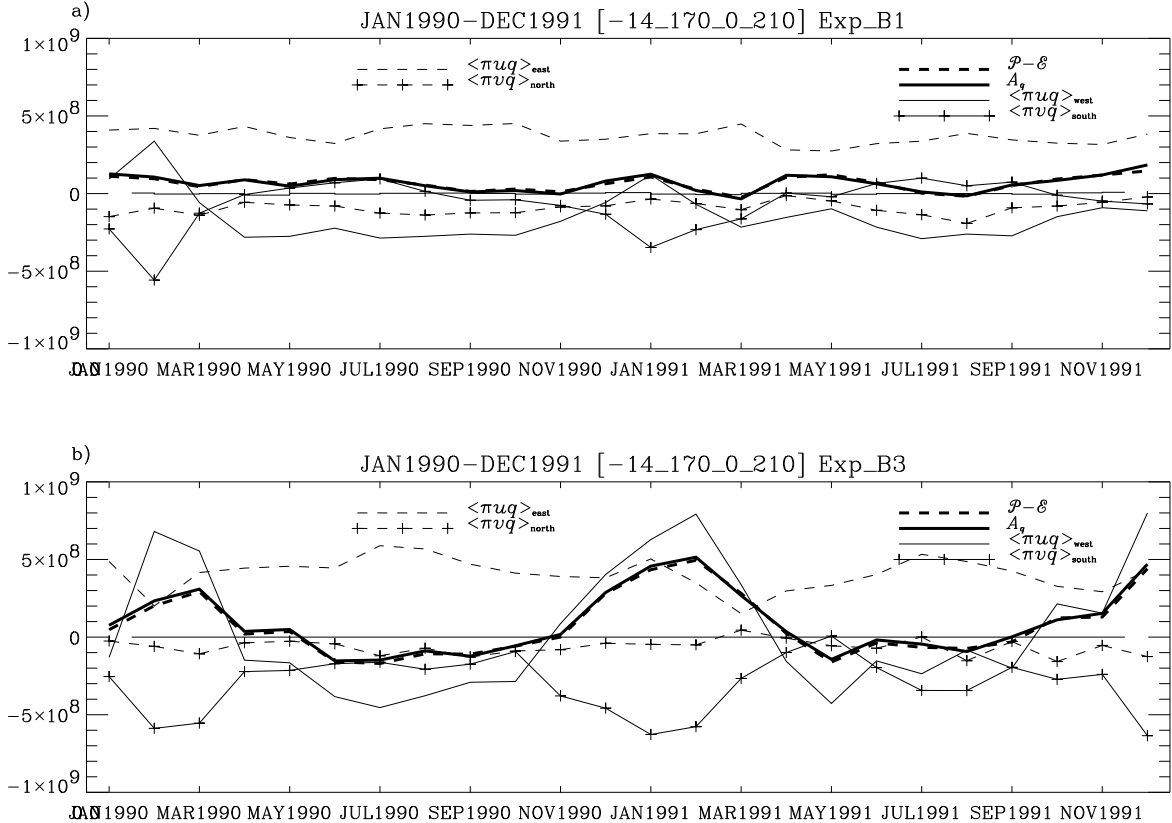


Figure 8: Monthly mean water vapor budget for Box S in; (a) Exp B1 and (b) Exp B3. Thick solid lines show sum of total, vertically-integrated horizontal fluxes (kg s^{-1}) through the four sides of the box. Thick dashed lines show net surface flux imbalance $\bar{P}_0 - \bar{E}_0$. Thin solid line shows flux entering through western edge of box $\langle \pi u q^\phi \rangle_{\text{west}}$. Note all fluxes have been defined such that positive values indicate inflow of water vapor. Thin dashed line indicates flux through eastern edge $\langle \pi u q^\phi \rangle_{\text{east}}$. Thin solid line with crosses indicates flux through southern edge $\langle \pi v q^\lambda \rangle_{\text{south}}$, and thin, dashed line with crosses indicates flux through northern edge $\langle \pi v q^\lambda \rangle_{\text{north}}$.

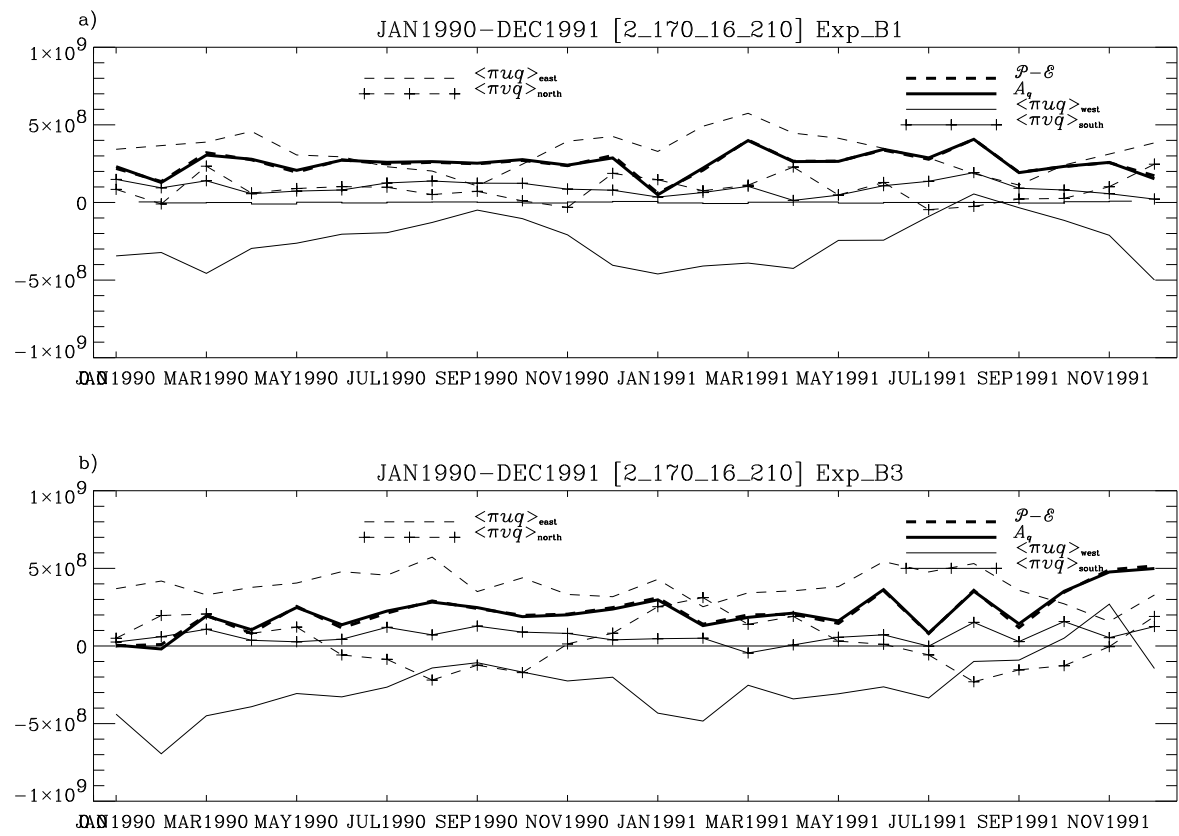


Figure 9: As in Figure 8 except for Box N.

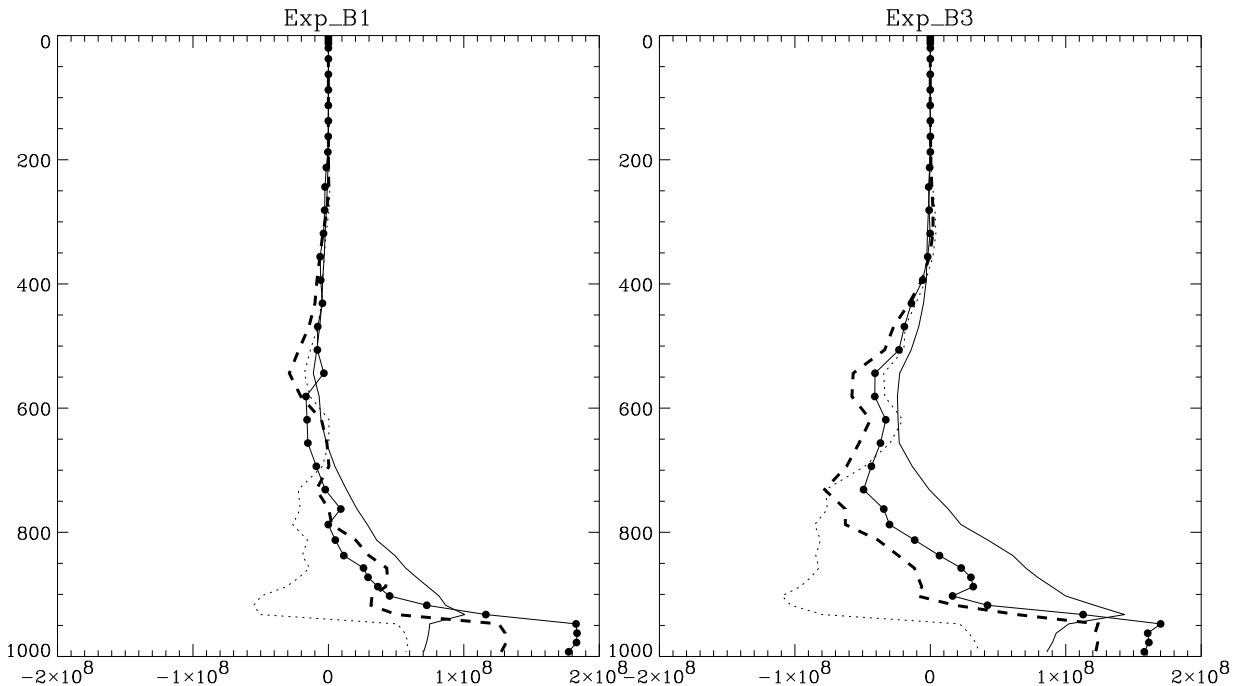


Figure 10: Box averaged profiles of water vapor flux quantities for JJA 1990 in Box S. Left panel shows results for Experiment B1 (weak re-evaporation), right panel for Experiment B3 (strong re-evaporation). Thin solid lines show $\langle \bar{\pi} u q^\phi \rangle_{\text{west}}^S - \langle \bar{\pi} u q^\phi \rangle_{\text{east}}^S$, thin dotted lines show $\langle \bar{\pi} u q^\lambda \rangle_{\text{south}}^S - \langle \bar{\pi} v q^\lambda \rangle_{\text{north}}^S$, and thick dashed lines show $\langle \bar{\pi} u q^\phi \rangle_{\text{west}}^S - \langle \bar{\pi} u q^\phi \rangle_{\text{east}}^S + \langle \bar{\pi} v q^\lambda \rangle_{\text{south}}^S - \langle \bar{\pi} v q^\lambda \rangle_{\text{north}}^S$, i.e., the net advective water vapor transport into Box S. The solid circles show the area integral of $q \vec{\nabla} \cdot (\pi \vec{V}_h)$, the component of the net transport into Box S accomplished by convergent winds.